Temperature-insensitive fiber-optic refractometer based on immobilization of polydimethilsiloxane film

Bing Sun*, *Member, IEEE*, Fei Li, Kandi Xu, Kaiming Zhou, and Zuxing Zhang

Abstract—A temperature-insensitive fiber refractometer, which consists of a simple single-mode–multimode–single-mode fiber optic scheme, is theoretically proposed and experimentally demonstrated. The multimode section is involved with a segment of D-shaped no core fiber (Ds-NCF) while the surface of the Ds-NCF is partially coated with a thin layer of polydimethylsiloxane (PDMS) film. Owing to the opposite thermo-optic coefficients (TOC) of the silica and the PDMS, a compact structure with nearly zero temperature dependence is fabricated. Moreover, such refractometer benefits from simplicity and low-cost and achieves competitive refractive index sensitivities of 140.1 nm/RIU in the range of 1.32 to 1.37, and 1147 nm/RIU over a RI range from 1.38 to 1.44. These excellent characteristics would find wide potential applications, such as chemical, biological, medical detection, and other fields.

Index Terms—Optical fiber sensors, Interferometers, Coatings, Refractive index, Temperature sensor

I. INTRODUCTION

TO date a variety of solutions have been developed for the fabrication of highly sensitive fiber-optic scheme, including offset-core fusion [1, 2], tapering [3, 4], chemical etching [5-6], side polishing [7-9], etc. For instance, Luo et al. reported a high RI sensitivity of 10777.8 nm/RIU when the fiber taper was working with the diameter of 4.6 μm around the RI of 1.3334 [10]. Additionally, multimode interference-based fiber RI sensors were reported in different structures [11-16]. However, the abovementioned fiber-optic refractive index sensors both involve a high temperature dependence with dozens of pm/°C, a corresponding temperature correction is required to overcome potential temperature fluctuation during RI sensing measurement.

Consequently, a periodically tapered photonic crystal fiber-based refractometer can obtain a significantly reduced temperature dependence of 8.4 pm/°C [17]. Wang et al. developed a low temperature cross-sensitivity RI sensor by exploiting the small thermal expansion coefficient of the simplified hollow-core photonic crystal fiber [18]. As an alternative, Li et al. present an intensity-modulated refractive index sensor based on an in-fiber Michelson interferometer, which the dip shifted toward a longer wavelength with a sensitivity of 0.048 nm/°C [19]. In addition, the hybrid LPG–FBG structures have been utilized for the RI sensing [20]. Although it shows low thermal sensitivities among these refractometers multiple disadvantages limit their applications. For instance, the flame-brushing technique or the offset-core fusion either require cost apparatus or show vulnerability, especially which the hydrofluoric is a corrosive and toxic material, easily leading to harm.

By contrast, D-shaped fibers that could be fabricated by means of removing the cladding entirely or partially maintains advantages of low manufacturing cost and easy fabrication, benefitting it to be a promising candidate to construct fiber-optic devices. Amid consisting of a flat polished surface can provide unlimited degrees of freedom for integrating various optical materials. Bao et al. observed a TM pass polarizing effect in metal-clad plasmon-assisted D-shaped fiber polarizers [21]. Lee et al. reported electrically manipulable in-line graphene devices by integrating graphene-based field effect transistors on a D-shaped fiber [22].

Here we take advantage of a conventional single-mode–multimode–single-mode fiber (SNS) structure to implement a temperature-insensitive refractometer, where the multimode section consists of a segment of D-shaped no core fiber (Ds-NCF), whereas a length of thin polydimethylsiloxane (PDMS) film (L_1) is immobilized on the polished surface of the Ds-NCF. It's worth noting that the PDMS film serves as a highly sensitive transparent material with a large negative thermo-optic coefficient (TOC, dn/dT of PDMS = -4.66×10^{-4} K^{-1}) and a refractive index of 1.4204 [23], whereas the original Ds-NCF share a positive TOC with the silica (dn/dT of silica = 9.2×10^{-6} K^{-1}). Thus, with an optimized thicknesses and lengths of the PDMS film, the platform can be functioned in a temperature-insensitive response. In order to verify the true action in our

Bing Sun, Fei Li, Kandi Xu, Zuxing Zhang are with the Advanced Photonic Technology Lab, College of Electronics and Optical Engineering, Nanjing University of Posts and Telecommunications, Nanjing 210023, China (e-mail: b.sun@njupt.edu.cn; lifei_798@163.com; 15162403928@163.com; zxzhang@njupt.edu.cn).

Bing Sun and Kaiming Zhou are with the Aston Institute of Photonic Technologies, Aston University, Birmingham B4 7ET, UK (e-mail: k.zhou@aston.ac.uk).

proposed scheme, an optimization procedure has been carried out in the two samples (sample #1 and sample #2). By taking the sample #2 as an example, the refractometer, accompanied with zero temperature response, has been experimentally fabricated with a maximal RI sensitivity of 1971 nm/RIU over a RI range from 1.40 to 1.44, respectively.

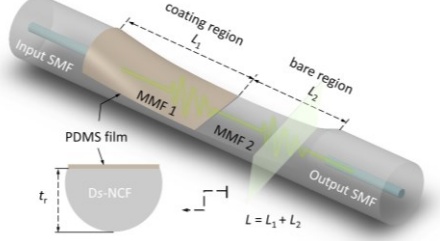## II. THEORETICAL SIMULATION AND EXPERIMENTAL DESIGN

Fig. 1. Schematic diagram of the proposed structure.

Figure 1 schematically shows the three-dimensional structure that consists of three sections: lead-in single-mode fiber (SMF), lead-out SMF, and the main multimode section. Here, the residual thickness of the Ds-NCF (see the inset in Fig. 1) is referred hereinafter as t_r, which can be decreased by prolonging the duration of polishing process. Thus, a length of the PDMS film (L_1) with a few microns thickness splits the Ds-NCF into two MMFs (e.g., the Ds-NCF coated with the PDMS film and the bare Ds-NCF) of appropriate lengths (L_1 and L_2) in series and of opposite temperature sensitivities. Initially, the incident light propagating in the fundamental mode along the lead-in SMF is efficiently coupled into the Ds-NCF, and the high-order modes, i.e. TE$_{0, n}$ or TM$_{0, n}$ modes are mainly excited through the coreless flat section due to the symmetry properties of the input field E$_{in}$ (r, θ) [24]. Whereas, the total phase difference ($\Phi(T, \lambda) = L_1\Delta\beta_1 + L_2\Delta\beta_2$) developed between the dominant modes, i.e. the j-th and k-th modes would be given by the following equation [25]:

$$\Phi(\lambda,\ T) = L_1\Delta\beta_1^{j,\ k} + L_2\Delta\beta_2^{j,\ k} \qquad (1)$$

where $\Delta\beta$ is the propagation constant. Thus, the condition for achieving zero temperature sensitivity is given by

$$\frac{\partial\Phi(\lambda,\ T)}{\partial T} = \frac{\partial(L_1\Delta\beta_1^{j,\ k} + L_2\Delta\beta_2^{j,\ k})}{\partial T} \qquad (2)$$

i.e.,

$$\Rightarrow \frac{\partial\Phi}{\partial T} = L_1(\alpha_1\Delta\beta_1^{j,\ k} + \frac{\partial\Delta\beta_1^{j,\ k}}{\partial T}) + L_2(\alpha_2\Delta\beta_2^{j,\ k} + \frac{\partial\Delta\beta_2^{j,\ k}}{\partial T}) \qquad (3)$$

Using $S_i = -(\alpha_i\Delta\beta_i^{j,\ k} + \partial\Delta\beta_i^{j,\ k} / \partial T) / (\partial\Delta\beta_i^{j,\ k} / \partial\lambda)$ (i=1, 2) , Eqs. (2) and (3) can be simplified as

$$\frac{\partial\Phi}{\partial T} = L_2(\ \eta S_1\frac{\partial\Delta\beta_1^{j,\ k}}{\partial\lambda} + S_2\frac{\partial\Delta\beta_2^{j,\ k}}{\partial\lambda}) \qquad (4)$$

where S_i represents the temperature sensitivities, η denotes the length ratio (L_1/L_2), and α_i are the coefficients of thermal expansion (CTE) corresponding to the two MMFs. It's worth noting that the bare Ds-NCF and the fused silica share the same CTE (e.g., α_2=5.7×10^{-7} K^{-1} over the temperature range of 0-200 °C), which can be omitted in contrast with its TOC. On the other hand, the contribution of the phase accumulation for the MMF1 originates from its TOC rather than its CTE (e.g., α_1) since the coating thickness of the PDMS film is thinner than several microns.
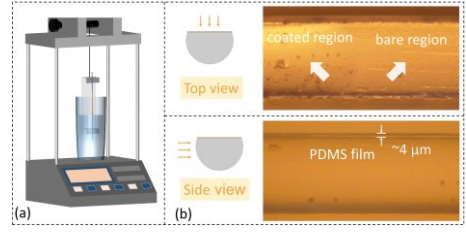

Fig. 2. (a) The employed dipping method, (b) the microscopy image of the structure on top view and side view.

In our experiment, we utilize a commercial arc fusion splicer (Furukawa S178) to fabricate the SNS structure, where the NCF employed is with a cladding diameter of D_c = 125 μm and a RI of 1.444 at λ = 1.55 μm. Thus, we take advantage of the home-developed fiber polishing system to obtain various Ds-NCFs with controllable residual thickness (t_r) and length (L). During the polishing process [26], the side view of the polished fiber was monitored by use of a microscope, and the residual thickness (t_r) of the D-shaped fiber was measured along the whole polished region. As shown in Fig. 2(a), a thin PDMS film has been immobilized on the flat surface of the Ds-NCF by the dip coating method, and then the whole fiber structure is rapidly solidified by means of placing it at 80 °C for 4 hours. It should be noted that the PDMS solution is prepared by means of mixing two precursors of silicone elastomer and curing agent with a 10:1 ratio, then leave it in a vacuum for 10 minutes to remove the bubbles. As a result of optimizing the dipping condition, i.e. the speed and the dipping time a well-designed PDMS film with thickness of a few microns can be immobilized on the flatness of the Ds-NCF. It can be seen from Fig. 2(b) that the coating region was speckled with particles, whereas the bare Ds-NCF shows smooth surface. In addition, we further verify thickness of the PDMS film was approximately 4 microns from the side view of the microscopy images. Thus, the film under various parameters would be considered and the appearance of the concerning film would be characterized by other techniques in the future work.

III. THEORETICAL SIMULATION AND EXPERIMENTAL DESIGN
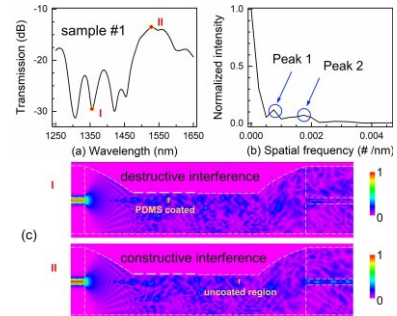
A. Temperature characteristics

Fig. 3. (a) Measured transmission spectrum of the sample #1. (b) The spatial frequency spectrum. (c) Beam propagation simulation.

Initially, the sample #1 with the residual thickness t_r = ~85 μm and the length L= ~5 mm has been fabricated. Thus, a PDMS film with thickness of several microns and length (L_1) of ~2.5 mm, corresponding to a ratio of 1, has been achieved. Thus, light from a broadband source with a low polarization spectral range of 1250 to 1650 nm, which the degree of

polarization is smaller than 10%, is launched and its transmission spectrum is recorded using an optical spectrum analyzer with a resolution of 0.02 nm. As shown in Fig.3 (a), the spectrum demonstrates a fringe pattern with multiple peaks and dips, indicating the power reaches minima and maxima along the transmission.

The operation involved in the proposed scheme can be described by means of the modal interference theory and expressed as

$$I = I_{core} + I_{clad} + 2\sqrt{I_{core}I_{clad}}\cos\Phi \quad (5)$$

where I_{core} and I_{clad} are the intensities of the core mode and cladding mode, respectively. And the phase difference can be considered through the differential modal group index [27] as

$$\Phi \approx \Phi_0 - \frac{2\pi\Delta\lambda}{\lambda_0^2}\Delta m_{eff}L, \text{ with } \Delta m_{eff} = \Delta n_{eff} - \lambda_0\frac{\partial}{\partial\lambda}\Delta n_{eff} \quad (6)$$

where the deviation from the center wavelength λ_0 is $\Delta\lambda = \lambda - \lambda_0$, the effective index difference is defined as $\Delta n_{eff} = n_{eff}^{clad1} - n_{eff}^{clad2}$.

The output light intensity presents minimums in the spectrum At the wavelength of 1306.4 nm (see point I), where $\Phi = (2m+1)\pi$, $m=0, 1, 2....$, the destructive interference occurs, as a result, the power reaches minimums while the wavelength of 1530.0 nm (see point II) corresponds to the constructive situation. Thus, its field evolution is also numerically simulated by a full-vectorial beam propagation method, as shown in Fig. 3(c). The spatial frequency spectrum, which is obtained by taking the FFT on the spectrum, is shown in Fig. 3(b).
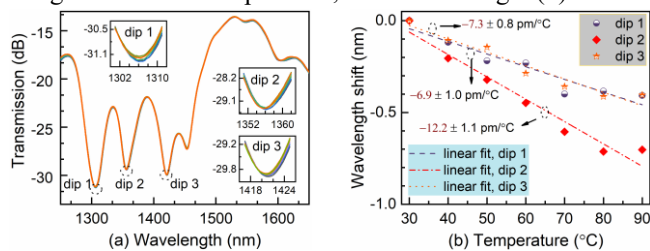

Fig. 4. (a) Measured transmission spectra of the sample #1. (b) Wavelength shifts of the three dips.

Furthermore, the spectra of the sample #1 placed in an oven with the temperature in the range from 30 to 90 ºC with an interval of 10 ºC is measured, where the three resonant dips (e.g., dip 1, dip 2 and dip 3) are particularly tracked in Fig. 4(a). It can be easily noticed from Fig. 4(b) that it yields temperature sensitivities of -6.9 ± 1.0 pm/ºC, -12.2 ± 1.1 pm/ºC and -7.3 ± 0.8 pm/ºC corresponding to the dip 1, dip 2 and dip 3. By contrast, we fabricated a bare Ds-NCF while its temperature dependence showed a 'red' shift of +63.8 ± 2.8 pm/ºC due to the positive TOC of silica, which is shown in Fig. 5. For comparison, sensitivities of the bare Ds-NCF and the proposed scheme are shown in the same ordinate, indicating the PDMS coated film plays parts. Moreover, the sensitivities are lower than that of the previously reported all-fiber refractometer with periodical tapers on a photonic crystal fiber [17]. This scheme is destined to accomplish the temperature-insensitivity response according to Eq. (4), and the structural optimization would be discussed in the next Section.

B. Refractive Index (RI) Measuring

In order to study the RI sensing response of the sample #1,

transmission spectra under analytes (standard RI liquids, Cargille Lab Inc.) with the RI from 1.30 to 1.44 are plotted in Fig. 6(a). We can easily observe that the whole spectra show changes while the three resonant dips move toward longer wavelengths, i.e. 'red' shift as the surrounding RI increases. As expected from the literature [28], the shifts follow a linear law in the low RI range, then an exponential trend in the whole RI range, the details of which is demonstrated in Figs. 6(b) and (c). For instance, the resonance (e.g., dip 1) demonstrates an average sensitivity of ~140.1 nm/RIU in the range of 1.32 to 1.37, thus, the sensitivity is significantly increased to be ~1147 nm/RIU at n=1.44. The RI sensitivity can be further improved along with the enhanced evanescent field as a result of optimizing the structural parameters, i.e. the residual depth.
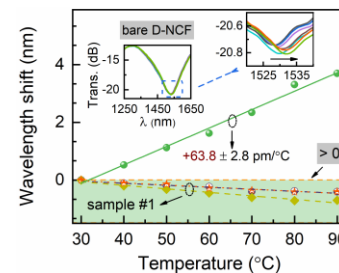

Fig. 5. Sensitivities of the bare Ds-NCF and the sample #1.
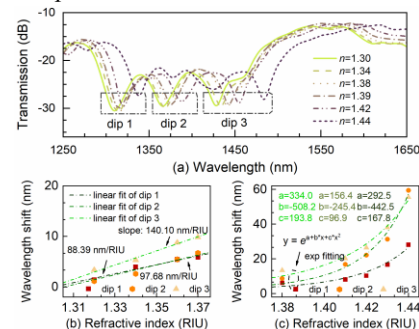
C. Structural Optimization

Fig. 6. (a) Measured spectral response at different surrounding RI. The dips wavelength shift versus the surrounding RIs ranging from 1.31 to 1.37 (b) and the RIs ranging from 1.38 to 1.44 (c).

The improved characteristics for temperature insenstivity and RI sensing can be developed by choosing the thickness of the residual depth and the coating length. As a result, another platfom (the sample #2) with t_r = ~68 µm and L = ~10 mm while the coating length (L_1) is approximately of 4 mm corresponding to a ratio of 0.67 has been employed. It's intuitively understood that the residual depth involving with the sample #2 allows for more contribution to the enhanced evanescent field, and then the improved RI sensitivities. As shown in Fig. 7(a), this sample also share the well-known interferometric theory, namely presenting multiple minimums and maximums along with the transmission spectrum. And there are also three similar resonance dips that can be found out for the sample #2. Here one of the dips (e.g., dip 2) is traced for the purpose of describing the relationship between the resonance dip and the surrounding RIs, which is plotted in Fig. 7(b). The corresponding RI response is exponentially fitting in the range of 1.38 to 1.44 RIU, and the maximal sensitivity can reach to be 1971 nm/RIU, resulting in a sensor resolution of 3.04×10^{-5} RIU condiering three times the maximum standard deviation

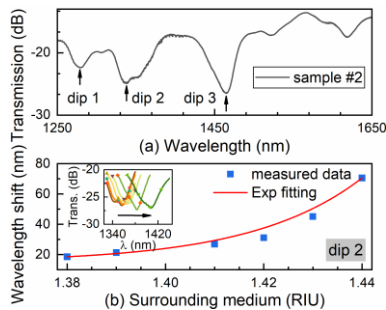obtained among all the experimental points [28].

Fig. 7. Measured dependencies of dip 2 wavelength corresponding to sample #2 with the surrounding refractive index.

Furthermore, such ratio (0.67) would solve the overloading suitation (e.g., the negative temperature sensitivity) involved in the sample #1. The dynamic balance with this length ratio could be artificially constructed due to the opposite temperature response of the PDMS film and the silica substrate. It can also be verified from Fig. 8 that the dips surely yield tiny temperature sensitivities of 0 ± 0.4 pm/ºC, -2.6 ± 1.9 pm/ºC and -7.0 ± 3.0 pm/ºC, respectively. We acknowledge that the dip 3 belongs to higher temperature sensitivity than another two dips (dip 1 and dip 2) as the longer wavelengths allow for more evanescent field enhancement.
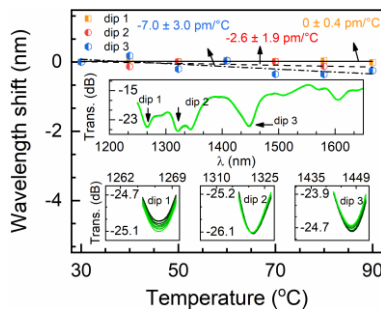

Fig. 8. Measured dependencies of dips wavelength vs the temperature with the sample #2.

IV. CONCLUSION

In summary, a compact refractometer consisting of the Ds-NCF coated with the PDMS film is theoretically proposed and experimentally investigated. A sensitivity of 140.1 nm/RIU in the range of 1.32 to 1.37. Significantly, the temperature-induced variations in the RI measurements can be very low. We believe that such low temperature dependence will find useful applications in fiber-optic refractometers.

REFERENCES

[1] Y. Zhao, X. G. Li, and L. Cai, "A highly sensitive Mach–Zehnder interferometric refractive index sensor based on core-offset single mode fiber," Sensors & Actuators A Physical **223**, 119-124 (2015).

[2] M. Q. Chen, H. M. Wei, Y. Zhao, X. H. Lei, and S. Krishnaswamy, "Temperature Insensitive Air-cavity Fabry-Perot Gas Pressure Sensor based on Core-Offset Fusion of Hollow-Core Fibers," Sensors and Actuators A Physical **298**, 111589 (2019).

[3] T. K. Yadav, R. Narayanaswamy, M, Bakar, Y. M. Kamil, and M. A. Mahdi, "Single mode tapered fiber-optic interferometer based refractive index sensor and its application to protein sensing," Optics Express **22**, 22802-22807 (2014).

[4] B. Sun, F. Fang, Z. Zhang, J. Xu, and L. Zhang, "High-sensitivity and low-temperature magnetic field sensor based on tapered two-mode fiber interference," Optics Letters **43**, 1311-1314 (2018).

[5] Y. Lei, H. Jie, X. Lan, H. Wang, and H. Xiao, "All-in-fiber optofluidic sensor fabricated by femtosecond laser assisted chemical etching," Optics Letters **39**, 2358-2361 (2014).

[6] F. Esposito, L. Sansone, A. Srivastava, F. Baldini, S. Campopiano, F. Chiavaioli, M. Giordano, A. Giannetti, A. Iadicicco, "Long period grating in double cladding fiber coated with graphene oxide as high-performance optical platform for biosensing," Biosens. Bioelectron. **172**, 112747 (2021)

[7] Z. Jiang, J. Dong, S. Hu, Y. Zhang, Y. Chen, Y. Luo, W. Zhu, W. Qiu, H. Lu, H. Guan, Y. Zhong, J. Yu, J. Zhang, and Z. Chen, "High-sensitivity vector magnetic field sensor based on side-polished fiber plasmon and ferrofluid," Optics Letters **43**, 4743-4746 (2018).

[8] F. Chiavaioli, P. Zubiate, I. Del Villar, C. Zamarreño, A. Giannetti, S. Tombelli, C. Trono, F. Arregui, I. Matias, and F. Baldini, "Femtomolar detection by nanocoated fiber label-free biosensors," ACS Sens **3**(5): 936–943 (2018).

[9] G. Moro, F. Chiavaioli, S. Liberi, P. Zubiate, I. Del Villar, A. Angelini, "Nanocoated fiber label-free biosensing for perfluorooctanoic acid detection by lossy mode resonance," Results opt. **5**: 100123 (2021).

[10] H. Luo, Q. Sun, X. Li, Z. Yan, Y. Li, D. Liu, and L. Zhang, "Refractive index sensitivity characteristics near the dispersion turning point of the multimode microfiber-based Mach–Zehnder interferometer," Optics Letters **40**, 5042-5042 (2015).

[11] F. Fang, B. Sun, Z. Zhang, J. Xu, and L. Zhang, "Improvement on refractive index sensing by exploiting the tapered two-mode fibers," Chinese Optics Letters **17**, 110604- (2019).

[12] T.-H. Xia, A. P. Zhang, B. Gu, and J.-J. Zhu, "Fiber-optic refractive-index sensors based on transmissive and reflective thin-core fiber modal interferometers," Opt. Commun. **283**(10), 2136–2139 (2010).

[13] Q. Liu and Q. Wang, "Refractive index sensor based on tapered PCF in-line interferometer," Chin. Opt. Lett. **10**, 090601-090601 (2012).

[14] Y. Zhao, L. Cai, X.-G. Li, F. Meng, and Z. Zhao, "Investigation of the high sensitivity RI sensor based on SMS fiber structure," Sens. Actuators A Phys. **205**, 186–190 (2014).

[15] D. Liu, A. K. Mallik, J. Yuan, C. Yu, G. Farrell, Y. Semenova, and Q. Wu, "High sensitivity refractive index sensor based on a tapered small core single-mode fiber structure," Opt. Lett. **40**(17), 4166–4169 (2015).

[16] Q. K. Wang, Y. Lingxin, F. Dang, Y. Xia, Y. Zhang, H. Zhao, Hu, and J. Li, "High sensitivity refractive index sensor based on splicing points tapered SMF-PCF-SMF structure Mach-Zehnder mode interferometer," Sens. Actuators B Chem. **225**, 213–220 (2016).

[17] P. Wang, L. Bo, C. Guan, Y. Semenova, Q. Wu, G. Brambilla, and G. Farrell, "Low-temperature sensitivity periodically tapered photonic crystal-fiber-based refractometer," Optics Letters **38**, 3795-3798 (2013).

[18] Y. Wang, D. N. Wang, C. Liao, T. Hu, J. Guo, and H. Wei, "Temperature-insensitive refractive index sensing by use of micro Fabry–Pérot cavity based on simplified hollow-core photonic crystal fiber," Optics Letters **38**, 269-271 (2013)

[19] Z. Li, Y. Wang, C. Liao, S. Liu, J. Zhou, X. Zhong, Y. Liu, K. Yang, Q. Wang, and G. Yin, "Temperature-insensitive refractive index sensor based on in-fiber Michelson interferometer," Sensors and Actuators B: Chemical **199**, 31-35 (2014)

[20] C. Trono, F. Baldini, M. Brenci, F. Chiavaioli, and M. Mugnaini, "Flow cell for strain- and temperature-compensated refractive index measurements by means of cascaded optical fibre long period and Bragg gratings,"Meas. Sci. Technol. **22**, 075204 (2011).

[21] Q. Bao, H. Zhang, B. Wang, Z. Ni, C. Haley, Y. Lim, Y. Wang, D. Tang, and K. Loh, "Broadband graphene polarizer," Nature Photonics **5**, 411–415 (2011).

[22] E. Lee, S. Choi, H. Jeong, N. Park, W. Yim, M. Kim, J. Park, S. Son, S. Bae, S. Kim, K. Lee, Y. Ahn, K. Ahn, B. Hong, J. Park, F. Rotermund, amd D. Yeom, "Active control of all-fibre graphene devices with electrical gating," Nature Communications **6**, 6851 (2015).

[23] C. He, J. Fang, Y. Zhang, Y. Yang, J. Yu, J. Zhang, H. Guan, W. Qiu, P. Wu, J. Dong, H. Lu, J. Tang, W. Zhu, N. Arsad, Y. Xiao, and Z. Chen, "High performance all-fiber temperature sensor based on coreless side-polished fiber wrapped with polydimethylsiloxane," Opt Express **26**, 9686-9699 (2018).

[24] H. Dong, L. Chen, J. Zhou, J. Yu, H. Guan, W. Qiu, J. Dong, H. Lu, J. Tang, W. Zhu, Z. Cai, Y. Xiao, J. Zhang, and Z. Chen, "Coreless side-polished fiber: a novel fiber structure for multimode interference and highly sensitive refractive index sensors," Opt. Express **25**, 5352-5365 (2017).

[25] S. Tripathi, A. Kumar, M. Kumar, and W. J. Bock, "Temperature insensitive single-mode–multimode–single-mode fiber optic structures with two multimode fibers in series," Opt. Lett. 39, 3340-3343 (2014).

[26] Y. Zhang, L. Wang, and Z. Liu, "The polishing detection method of side-polished fiber", Proc. SPIE 8202, 2011 International Conference on Optical Instruments and Technology: Solid State Lighting and Display Technologies, Holography, Speckle Pattern Interferometry, and Micro/Nano Manufacturing and Metrology, 820211 (2011).

[27] B. H. Lee, and J. Nishii, "Dependence of fringe spacing on the grating separation in a long-period fiber grating pair," Appl. Opt. 38, 3450-3459 (1999).

[28] F. Chiavaioli, C. A. J. Gouveia, P. A. S. Jorge, F. Baldini, "Towards a Uniform Metrological Assessment of Grating-Based Optical Fiber Sensors: From Refractometers to Biosensors," Biosensors 7(2): 23 (2017).